Iron environment in pseudomorphic iron silicides epitaxially grown on Si(111)

C. Pirri, M. H. Tuilier, P. Wetzel, S. Hong, D. Bolmont, and G. Gewinner
Laboratoire de Physique et de Spectroscopie Electronique, Faculté des Sciences et Techniques 4, rue des Frères Lumière, 68093 Mulhouse Cédex, France

R. Cortès and O. Heckmann
Laboratoire pour l'Utilisation du Rayonnement Electromagnetique, Université de Paris-Sud, 91405 Orsay Cédex, France

H. von Känel
Laboratorium für Festkörperphysik, Eidgenössische Technische Hochschule Zürich, 8093 Zürich, Switzerland
(Received 26 July 1994; revised manuscript received 18 October 1994)

Pseudomorphic iron-silicide phases grown on Si(111) have been studied by means of low-energy electron-diffraction, x-ray photoelectron-diffraction, and surface extended x-ray-absorption fine-structure experiments at the Fe K edge (7110 eV). These silicides have been epitaxially grown by codeposition of Fe and Si onto a room-temperature Si(111) substrate with silicide stoichiometry ranging from FeSi to $FeSi_x$ ($x \sim 2$). In all cases, they were found to be epitaxial as attested to by a (1×1) low-energy electron-diffraction pattern observed after room-temperature deposition. X-ray-absorption measurements reveal that Fe atoms are coordinated with eight Si atoms for all metastable silicides with bond lengths of 2.34–2.37 Å and with Fe atoms with bond lengths in the 2.68–2.75-Å range. Fe-Si and Fe-Fe bond lengths as well as coordination numbers are found to increase with Fe contents within the silicide. These experiments confirm the formation of an epitaxial cubic and metastable CsCl-type FeSi upon deposition of Fe and Si in the 1:1 ratio onto a room-temperature Si(111) substrate. Furthermore, all data recorded from $FeSi_2$ grown at room temperature or annealed at high temperature, are consistent with CsCl-derived or α-derived $FeSi_2$ structures. Finally, the present data are inconsistent with the formation of a CaF_2-type $FeSi_2$ structure.

I. INTRODUCTION

The study of Fe silicide growth on Si(111) has stimulated renewed interest in recent years. This interest was due mainly to the possible growth of the semiconducting β-$FeSi_2$ phase on Si(111) which could be used as a constituent of Si-based optoelectronic devices. The Fe silicide/Si(111) interface has been extensively studied using various experimental techniques, and numerous silicide phases have been identified. Most of them have bulk counterparts, such as semiconducting ε-FeSi,[1] metallic α-derived $FeSi_2$,[2–5] DO_3-type Fe_3Si,[6] and semiconducting β-$FeSi_2$.[1,7–15] Furthermore, metastable Fe silicides without bulk counterparts can be grown on Si(111). A CaF_2-type $FeSi_2$ (γ-phase) has been reported for very thin Fe deposits on Si(111) in the 3–5-Fe-monolayer range.[16–18] Alternatively the γ phase may be formed during a melting-recrystallizing process of β-$FeSi_2$.[19] Finally cubic CsCl-derived and tetragonal α-$FeSi_2$-derived silicides are observed during Fe/Si(111) interface formation.[20–23] The cubic phases can also be synthesized by molecular-beam epitaxy (MBE). At composition 1:1, a FeSi phase is epitaxially grown on Si(111) and is stable up to a critical thickness of ~25 Å. For larger thicknesses, FeSi is observed in a metastable form up to about 1000 Å when grown on a room-temperature (RT) substrate. Upon annealing above 300 °C, this CsCl-type FeSi phase transforms into the bulk ε-FeSi phase.[24,25] Cubic $Fe_{1-x}Si$ ($x \sim 0.5$) is formed either by annealing thin (<15 Å) CsCl-type FeSi films or by molecular-beam epitaxy in a composition varying from 1:1 to 1:2. The formation of such pseudomorphic $Fe_{1-x}Si$ phases is interesting *per se*, but also for technical applications since it was found that different epitaxial orientations of β-$FeSi_2$ on Si(111) are observed through the pseudomorphic to stable $FeSi_2$ transition starting with $Fe_{1-x}Si$.[25] It was proposed that cubic $Fe_{1-x}Si$ ($0<x<0.5$) is derived from the CsCl-FeSi phase by forming randomly distributed Fe vacancies within the silicide which preserve the CsCl crystal symmetry and stoichiometry (Fig. 1). The γ-$FeSi_2$ structure can also be deduced form the CsCl one by removing every nearest Fe-atom neighbor of a given Fe atom, thus making periodically (instead of randomly) ordered Fe vacancies. On the other hand, recent x-ray-diffraction experiments[4] performed on metal-organic chemical-vapor-deposited $FeSi_2$ films have shown that grains with α-$FeSi_2$-derived phase are formed. The α-$FeSi_2$ bulk phase is only observed at high temperature ($T>940$ °C) with lattice parameters $a=2.695$ Å and $c=5.134$ Å. Metastable α-$FeSi_2$ epitaxially grown on Si(111) at ~500 °C is derived from the bulk one with some atomic rearrangements. Indeed a distribution of the Fe atoms was proposed, introducing additional (001) Fe planes in an intermediate position (Fig. 1) at $c/2$. To preserve the $FeSi_2$ stoichiometry, occupation factors of $\frac{1}{6}$ and $\frac{5}{6}$ have been considered for the intermediate and the other (001) Fe

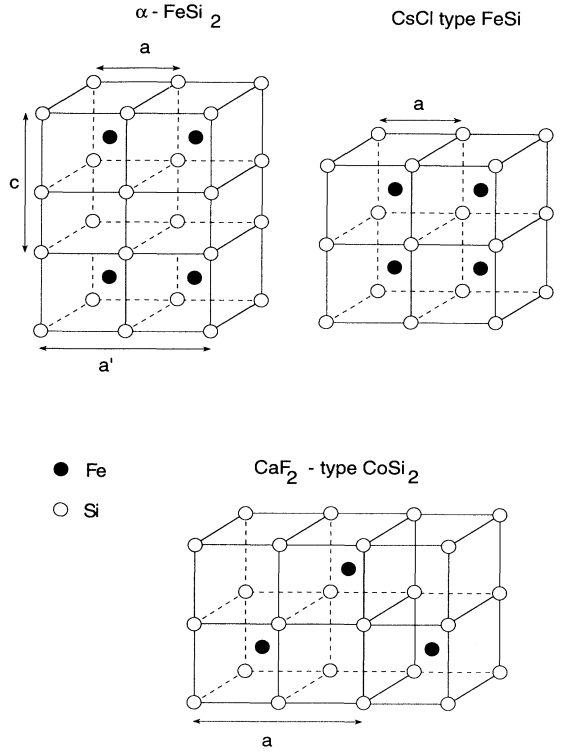

FIG. 1. Structure of CsCl-type FeSi, tetragonal α-$FeSi_2$, and CaF_2-type $CoSi_2$.

planes, respectively.

This paper deals with structural characterization of RT-grown and high-temperature-annealed Fe silicides using elastic low- and inelastic medium-energy electron-diffraction (LEED and IMEED), x-ray photoelectron-diffraction (XPD) and extended x-ray-absorption fine-structure (EXAFS) measurements on pseudomorphic MBE-grown Fe silicides on Si(111).

II. EXPERIMENT

Pseudomorphic $FeSi_x$ $(1<x<2)$ silicides were prepared in an UHV system with a base pressure of 8.10^{-11} mbar by codeposition of Fe and Si onto a Si(111) 7×7 substrate held at RT. Fe (Co) and Si were evaporated from boron nitride and carbon crucibles, respectively, at stable and reproducible rates in the 1–2-Å/min range. These low evaporation rates, checked independently for Si and Fe (Co) using quartz-crystal microbalances, allowed the fabrication of silicides with well-controlled stoichiometry. Epitaxial Fe silicide layers with thicknesses in the 30–90-Å range were prepared by RT codeposition of Fe and Si in the desired stoichiometry onto a 6-Å-thick $FeSi_2$ template. This codeposited template was annealed at 500 °C. Some of these silicides have been annealed in the RT–600 °C temperature range. A 90-Å-thick $CoSi_2$ layer was also epitaxially grown on Si(111) by codeposition of Co and Si in a 1:2 ratio, and annealed at 550 °C. This $CoSi_2$ layer is used as a reference for the EXAFS data treatments. Additionally, 50-Å-thick FeSi and $FeSi_2$ (so-called $Fe_{0.5}Si$ in Ref. 25) epitaxially grown on Si(111) in the Laboratorium Für Festkörperphysik (ETH Zürich) have been examined by EXAFS. These layers were also grown by codeposition of Fe and Si.

The silicide crystallinity was checked using LEED optics working in both low-energy (<200 eV) and medium-energy (~1000 eV) electron modes. At low electron energy, the diffraction pattern is very surface sensitive and arises from electrons coherently backscattered by large ordered domains (>100 Å), while at medium-electron energy a less energy-dependent diagram is observed (for ordered epitaxial layers). This diagram arises from incoherently backscattered electrons and exhibits angular distributions very similar to that of Auger or x-ray photoelectrons.[26] As opposed to these last techniques, IMEED is not atom specific, but provides structural information similar to that possessed by secondary electrons that originate at point sources within the sample. IMEED is much more bulk sensitive than LEED, and the coherence length is of the order of the inelastic electron mean free path (~10–20 Å), like for Auger-electron or x-ray photoelectron diffraction. Thus by working in the IMEED mode, the structural information is more local than in LEED. Finally, structural information gained from IMEED is somewhat less quantitative than XPD, especially in a precise determination of the polar and azimuthal forward-scattering directions, but it very quickly gives an indication of epitaxy, crystal symmetry, and order.

X-ray photoelectron diffraction experiments were performed *in situ* with an angle-resolved multidetection spectrometer using Al $K\alpha(\hbar\omega=1486.6$ eV) radiation. The angle of acceptance of the photoelectron analyzer was set to $\pm1°$. After LEED and XPD measurements, a 20-Å-thick protective amorphous Si capping layer was deposited onto the silicide film. EXAFS measurements were performed at the Laboratoire pour l'Utilisation du Rayonnement Electromagnetique (LURE) at Orsay either on the surface EXAFS setup installed on the wiggler beam line or on the x-ray-absorption spectroscopy (XAS 2) beam line of the DCI storage ring. In the former, the incident radiation was monochromatized using a Si(311) focusing two-crystal spectrometer, while a Si(111) plane two-crystal spectrometer was used in the latter. Both beam lines are equipped with a mirror at glancing incidence for the harmonic rejection. The variation of the x-ray-absorption coefficient was measured above the K edge of iron (7111 eV) and cobalt (7766 eV) at RT in the fluorescence mode. The data were collected at different angles ψ between the electric field or polarization vector of the synchrotron radiation and the normal to the sample. In the fluorescence detection mode, the penetration depth of the photon is larger than the silicide thickness, and thus intense Bragg diffraction beams are generated in the Si(111) substrate. They generally contribute to the absorption spectrum as high peaks (glitches). For EXAFS spectra recorded on the XAS2 beam line, these Bragg-reflection-related peaks are detected at any angle of incidence ψ of the light. These Bragg reflection peaks

were removed by substituting the region of the spurious peak by the same energy range collected at an angle ψ shifted by a few degrees. The small angle of acceptance of the energy resolved fluorescence detector used in the SEXAFS setup allows us to eliminate these Bragg reflection peaks from the silicon substrate by using properly chosen angles of incidence of the light. (In practice, the spectra were recorded at $\psi \pm 1°$.)

III. RESULTS AND DISCUSSIONS

A. XPD, LEED, and IMEED results

Silicide deposited in a 1:1 ratio results in a well-ordered FeSi phase, as attested by a 1×1 LEED pattern with well-defined threefold symmetry. Diffraction spots are sharp, showing the formation of large FeSi domains epitaxially grown on Si(111). At higher electron energy ($\sim$1000 eV) a well-contrasted IMEED diagram is observed with strong intensity modulations versus position on the fluorescent screen. It reflects the strong emission anisotropy versus angle of electron emission. The solid angle intercepted by the screen is large enough to analyze electrons emitted with polar angles in the $-40°,+40°$ range. The intensity is mainly enhanced along the axis corresponding to the dense $(1\bar{2}1)$- and $(\bar{1}01)$-type planes in real space. As for LEED, the IMEED pattern shows a threefold symmetry evidenced by different intensity modulation versus polar angle along opposite $[1\bar{2}1]$ and $[\bar{1}2\bar{1}]$ azimuthal directions. Along a given crystallographic direction the intensity variation is very similar to that observed for epitaxially grown $CoSi_2$ showing that the crystal symmetry deduced from IMEED is nearly cubic. Angular positions of the intensity maxima are quite consistent with those measured using XPD on nearly cubic thin Fe silicides, and indicate that FeSi domains are essentially of B type when grown on Si(111).[23] Such LEED and IMEED patterns are preserved when the Fe content in the silicide is decreased down to a value corresponding to a 1:1.6 stoichiometry ratio. When the silicide stoichiometry is close to 1:2, the low-energy pattern consists of large spots superimposed on a diffuse background. A degradation of the $FeSi_x$ ($x\sim2$) diffraction pattern, with respect to the FeSi one, has also been observed by reflection-high-energy electron-diffraction (RHEED) measurements.[25] However, the higher electron energy IMEED diagram is still visible. Figure 2 shows the Fe $2p_{3/2}$ ($Ec=779$ eV) core-level intensity versus polar angle along the $[\bar{1}2\bar{1}]$ symmetry line of the silicon substrate measured for FeSi and $FeSi_x$ ($x\sim2$) grown at RT. XPD profiles are very similar in both compounds. This figure clearly shows that the intensity modulation is preserved when the silicide stoichiometry is changed from 1:1 to 1:2, indicating that structural order at a few tens of Å scale as well as epitaxy are preserved. Single-oriented B-type domains are also formed for the 1:2 stoichiometry. Furthermore, XPD profiles suggest that the structure of FeSi and $FeSi_x$ ($x\sim2$) are very close, and similar to those proposed in Ref. 25. At this stage, XPD, LEED, and IMEED show that epitaxial Fe silicides can be grown at RT on Si(111).

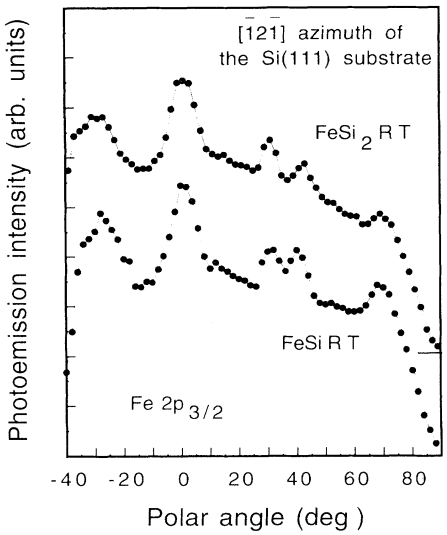

FIG. 2. Experimental polar-angle scans of Fe $2p_{3/2}$ emission for 90-Å-thick codeposited $FeSi_x$ ($x\sim2$) and FeSi, epitaxially grown at RT on Si(111), along the $[\bar{1}2\bar{1}]$ azimuth of the Si(111) substrate. The polar angle $\theta=0°$ corresponds to the normal emission.

Upon annealing FeSi and $FeSi_x$ ($x\sim2$) layers at 500 °C, LEED and IMEED diffraction patterns completely disappear, leaving only a strong diffuse background. This evolution is due to a phase transition toward stable bulk ε-FeSi and β-$FeSi_2$ phases.[13,24,25] In particular, their valence-band evolution upon annealing clearly demonstrated the FeSi ($FeSi_2$) phase transition toward ε-FeSi (β-$FeSi_2$).[13] Pseudomorphic FeSi layers with thicknesses larger than 15 Å undergo a transition toward the stable bulk phase, namely ε-FeSi, when the annealing temperature is above 300 °C. This phase is epitaxial for thicknesses in the 15–25-Å range, and polycrystalline above 25 Å.[25] The 90-Å-thick pseudomorphic FeSi layer considered in this work transforms into polycrystalline ε-FeSi upon annealing, as attested by LEED and IMEED. Codeposited $FeSi_x$ ($x\sim2$) films transform into either epitaxial or polycrystalline β-$FeSi_2$, depending on the film thickness. Upon annealing at 500 °C, 90-Å-thick $FeSi_x$ ($x\sim2$) layers are transformed into polycrystalline β-$FeSi_2$. This situation is quite different for thinner Fe disilicides prepared in a Fe-to-Si ratio close to 1:2. Upon annealing a 30-Å-thick silicide at 500 °C, a sharp 2×2 LEED pattern along with a well-contrasted IMEED diagram are observed. The IMEED diagram and XPD profiles are quite similar to those measured for thicker RT-grown FeSi and $FeSi_x$ ($x\sim2$) layers. The main difference between annealed and RT-grown $FeSi_x$ ($x\sim2$) silicide XPD profiles is an improvement of the contrast. For thin films, the IMEED diffraction patterns are unaffected for annealing temperatures as high as 600 °C, and thus the nearly cubic crystal symmetry inferred from both IMEED and XPD is common to all pseudomorphic Fe silicides presented in this work.

B. EXAFS results and data analysis

The data were analyzed using the software "EXAFS pour le Mac."[27] After background subtraction and normalization to the edge jump, the data were k^2 weighted and Fourier transformed between 3 and 12 $Å^{-1}$. The $k\chi(k)$ data recorded from pseudomorphic Fe silicides and from the reference compounds $CoSi_2$, β-$FeSi_2$, and ε-FeSi are compared in Fig. 3. The corresponding Fourier transforms (FT's) are shown in Figs. 4 and 5. At a given stoichiometry, EXAFS measured on 90- and 50-Å-thick silicide layers yield very similar results, considered in detail in the following discussion.

$CoSi_2$ crystallizes in the CaF_2 structure with a unit-cell length of 5.368 Å. Co atoms are surrounded by eight first-shell Si neighbors at a distance of 2.324 Å, and 12 second-shell Co neighbors at 3.794 Å. These two neighbor shells are clearly visible in the FT on Fig. 4. Polycrystalline β-$FeSi_2$ and ε-FeSi were obtained by annealing at 500 °C RT-grown $FeSi_2$ and FeSi layers, respectively. β-$FeSi_2$ crystallizes in an orthorhombic structure with lattice parameters $a=9.863$ Å, $b=7.791$ Å, and $c=7.833$ Å.[28] This structure is rather complicated, since two kinds of Fe sites contribute to the EXAFS signal. There are Fe-Si distances stretching from 2.333 to 2.437 Å with a mean value of 2.37 Å and two Fe atoms at 2.967 Å. The FT of β-$FeSi_2$ data shows essentially a main peak of the first Si neighbor's shell. ε-FeSi crystallizes in a perfect cubic lattice. The nearest-neighbor (NN) environment of Fe is one Si at 2.305 Å, three Si atoms at 2.353 Å, and three Si atoms at 2.495 Å. The shortest Fe-Fe bond length is 2.756 Å.[28] The FT spectrum of Fig. 5 clearly shows a contribution from these Fe-Si and Fe-Fe bond lengths, in agreement with previously published data.[29]

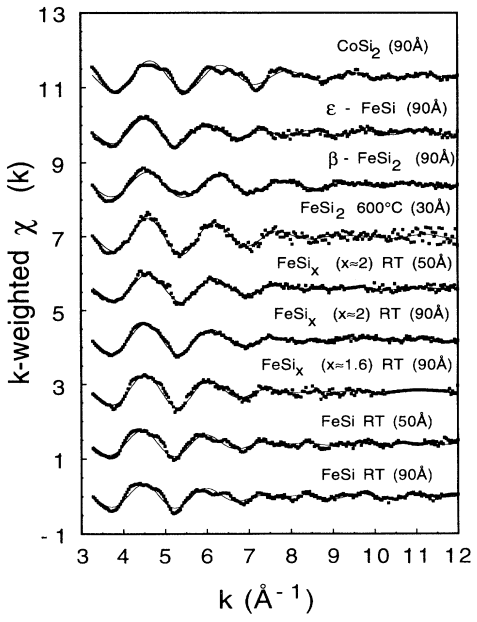

FIG. 3. k-weighted $\chi(k)$ EXAFS data (dots) recorded at normal incidence ($\psi=90°$) of $CoSi_2$ at the Co K edge, and at the magic incidence ($\psi=54°$) of epitaxial Fe silicides β-$FeSi_2$ and ε-FeSi at the Fe K edge. Also shown are the Fourier-filtered contribution of Si NN and Fe NNN (full line).

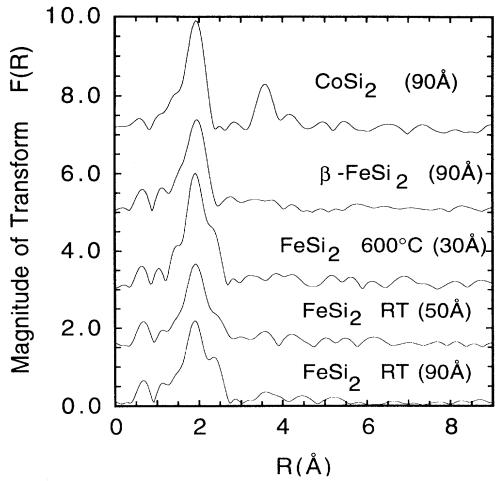

FIG. 4. Fourier transform magnitude $F(R)$ of Fe and Co EXAFS for epitaxial Si rich iron silicides β-$FeSi_2$ at magic incidence of the light ($\psi=54°$), and $CoSi_2$ at normal incidence ($\psi=90°$).

As opposed to $CoSi_2$ and β-$FeSi_2$, the first neighbor's contribution in pseudomorphic Fe silicides is split in two subshells in the 2–3-Å region. The presence of these two subshells is independent of the silicide stoichiometry. They are attributed to Si NN and Fe next-nearest neighbors (NNN). It is noteworthy that in any metastable Fe silicides, Fe atoms are bound to Si and Fe atoms with bond lengths shorter than ~3 Å. The formation of large $FeSi_2$ domains with a CaF_2-type structure, the so-called γ-$FeSi_2$ structure, can be safely ruled out for Fe silicides presented in this work. The Fourier-filtered contribution of NN and NNN peaks are superimposed on the experi-

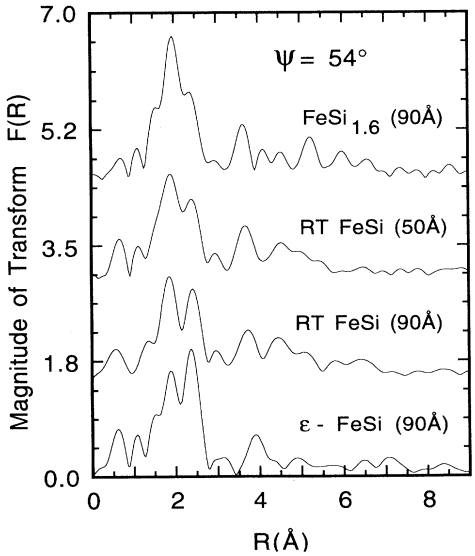

FIG. 5. Fourier transform magnitude $F(R)$ of Fe EXAFS for epitaxial Fe-rich iron silicides and ε-FeSi at magic incidence of the light ($\psi=54°$).

mental data in Fig. 3, and have been simulated in the single-scattering formalism using theoretical[30] and experimental ($CoSi_2$ and Co metal) phase shifts and backscattering amplitudes. In the present case the distances of Fe atoms to the Si NN and Fe NNN are very close and unresolved in the FT. Thus simulations must be performed by a two-shell fit, introducing numerous fit parameters. In order to minimize the number of parameters which are allowed to vary during the simulation, some of them have been extracted from reference compounds. In particular, an accurate determination of the threshold energy E_0 becomes of crucial importance. E_0 has been fixed using the Lee and Beni method,[31] which requires that the imaginary part and absolute value of the FT peak at the same distance for a given set of phase shifts. E_0 has been adjusted only within ± 2 eV around the value measured for model compounds β-$FeSi_2$ and UFe_2Si_2 (Ref. 22 and references therein) for Si and Fe, respectively.

Furthermore the accuracy of the difference between Fe-Si and Fe-Fe bond lengths has been improved using the beat node method.[32,33] This method has been used fruitfully for a similar system.[34] Figure 6 shows the Fourier-filtered amplitude for the pseudomorphic Fe silicides as a function of the electron wave vector k. Well-defined null minima are clearly detected, indicating that for any RT-grown silicide the FT peak in the 2–3-Å range corresponds only to two first-neighbor subshells. Furthermore, Fig. 6 shows that the difference between Fe-Si and Fe-Fe bond lengths changes significantly versus silicide stoichiometry. This difference increases as a function of Fe enrichment of the silicide grown at RT. The lowest difference is measured for $FeSi_2$ annealed at 600 °C. A rather good estimation of Fe-Si and Fe-Fe bond-length differences can be extracted from data in Fig. 6. Since, in this case, the backscatterers are different, an accurate determination of the Fe-Si and Fe-Fe scattering phase shifts at a given k value is required.

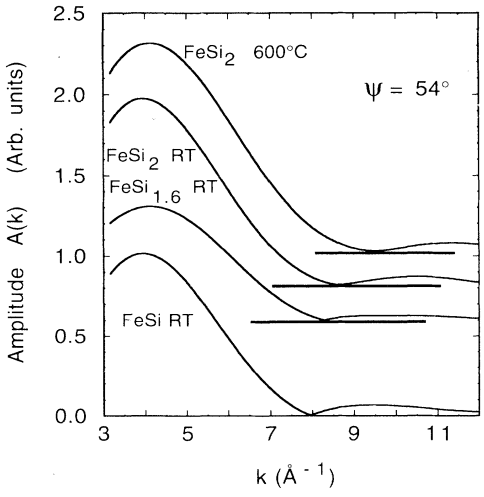

FIG. 6. Amplitude functions $A(k)$ of the Fourier-filtered contribution of Si NN and Fe NNN for the 90-Å-thick RT codeposited Fe silicides, and for a 30-Å-thick codeposited $FeSi_2$ layer annealed at 600 °C.

The use of bulk ε-FeSi and β-$FeSi_2$ as reference compounds is not desirable since the first Fe-Si distances are spread over a wide range of 0.19 and 0.11 Å, respectively. Thus we used $CoSi_2$ and Co metal as model compounds.

Phase shifts have been extracted from EXAFS data measured on $CoSi_2$ epitaxially grown on Si(111) with the same thickness as pseudomorphic Fe silicides in order to minimize thickness-dependent effects in the data. When epitaxially grown on Si(111), the $CoSi_2$ film is under tensile strain due to the mismatch of about -1.2% between Si and $CoSi_2$ lattice parameters. The morphology of $CoSi_2$ layer epitaxially grown on Si(111) has been studied extensively by von Känel.[35] Rutherford backscattering (RBS) and transmission electron microscopy (TEM) experiments discussed in Ref. 35 show that codeposited $CoSi_2$ layers are never really coherent with the substrate when epitaxially grown on Si(111) with a B-type interface. However, it was found that, above 40–45 Å, a substantial increase of dislocation occurs within the film. The parallel strain was deduced from RBS by measuring the angular shift $\Delta\theta$ between the [110] channeling direction in the silicide and the [114] direction of the substrate. $\Delta\theta$ measured by von Känel on numerous thin codeposited $CoSi_2$ layers annealed at 500–600 °C are typically in the $-0.33°, -0.46°$ range. $\Delta\theta$ would be of zero for a fully relaxed layer. From elastic constant determinations, a $\Delta\theta$ of $-0.59°$ would be measured for a perfect coherent $CoSi_2$ layer.[35] Thus the Co-Si bond lengths measured by EXAFS would be between that expected for a perfect CaF_2-type lattice and that of a fully strained layer. It is 2.324 Å for a perfect $CoSi_2$ [$a = 5.367$ Å (Ref. 28)] crystal, and the mean Co-Si bond length would be about 2.335 Å for a $CoSi_2$ layer, coherently matched to the substrate. These bond lengths are very close (at the EXAFS scale) and within the experimental EXAFS bond length error. However, slight differences between EXAFS data measured on epitaxial layers at grazing and normal incidences of the light are expected. Indeed, in a trigonally distorted lattice, a $\Delta\theta$ of $-0.59°$ would give rise to two different Co-Si bond lengths. A given Co atom would be surrounded by six Si atoms at 2.35 Å with

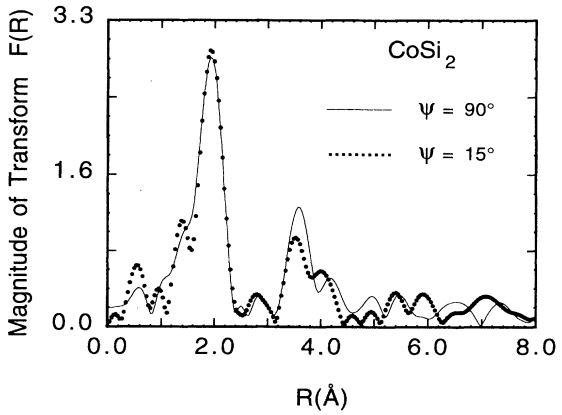

FIG. 7. Fourier transform magnitude $F(R)$ of Co EXAFS for a 90-Å-thick $CoSi_2$ layer epitaxially grown on Si(111), measured at grazing ($\psi = 15°$) and normal ($\psi = 90°$) incidences.

TABLE I. Structural parameters determined from SEXAFS at the Co K edge of $CoSi_2$ for the first coordination shell.

	Pair	R (Å)	N^*	σ (Å)
$CoSi_2$ $\psi=90°$ normal incidence	Co-Si	2.33±0.02	8.4±0.5	0.070
$CoSi_2$ $\psi=15°$ grazing incidence	Co-Si	2.33±0.02	7.6±0.5	0.078

bond angles of 70.9° (with respect to the surface normal), and two Si atoms at 2.30 Å with Co-Si bonds perpendicular to the surface. Anisotropy effects due to the strain have been tested by comparing the 90-Å-thick $CoSi_2$ EXAFS data collected at normal ($\psi=90°$) and grazing incidences ($\psi=15°$). The relevant FT's are compared in Fig. 7, and simulation results are summarized in Table I. Simulation results show only very small differences between Co-Si distances and coordination numbers extracted from normal- and grazing-incidence spectra. The Co-Si bond length is found to be 2.33 Å in both incidences, indicating that the $CoSi_2$ layer anisotropy is very weak.

The phase shifts and backscattering amplitudes extracted from $CoSi_2$ recorded at grazing incidence have been used in the calculations for the Fe-Si pair. Phase shifts and backscattering amplitudes extracted from Co-metal data have been used for the Co-Co pair. The accuracy of the beat node method can be estimated if the difference between Co-Si and Co-Co phase shifts is compared to the difference between calculated Fe-Si and Fe-Fe backscattering phase shifts at a given k value. In doing so we found that in the range of the amplitude minima observed for the Fe silicide films, the phase-shift difference $\Delta\phi$ are close to π and amount to 3.0±0.1 and 3.2±0.2 rad at 7.5 and 9.5 $Å^{-1}$, respectively, depending on the phase shifts used (theoretical or $CoSi_2$ extracted). The results of the simulations along with that of the beat node method are summarized in Table II. Figure 8

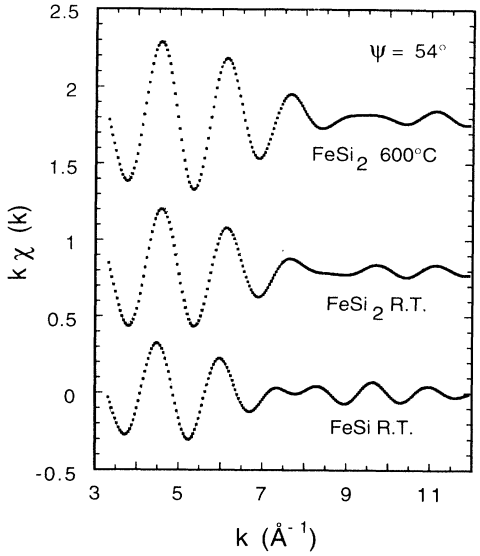

FIG. 8. Representative fits (full line) to the Fe K EXAFS data (dots) for 90-Å-thick RT-grown FeSi and $FeSi_x$ ($x\sim2$) layers, and for a 600 °C annealed $FeSi_2$ layer (30 Å).

TABLE II. Structural parameters deduced from the analysis of EXAFS spectra recorded at the Fe K edge ($\psi=54°$) from codeposited iron silicides epitaxially grown on Si(111). $\Delta\sigma$ is related to Co-Si and Co-Co bonds in $CoSi_2$ and Co metal, respectively. In the last column, ΔR_{BN} is the difference between the Fe-Fe and Fe-Si bond lengths, determined using the beat node method.

	Pair	R (Å)	N	$\Delta\sigma$ (Å)	ΔR_{BN} (Å)
$FeSi_2$ (annealed at 600 °C) 30 Å	Fe-Si	2.35±0.02	8±0.5	0	0.33±0.02
	Fe-Fe	2.68±0.02	3±0.5	0	
$FeSi_2$ (RT depostied) 50 Å	Fe-Si	2.35±0.02	8±0.5	0.04	0.34±0.02
	Fe-Fe	2.69±0.02	3.1±0.5	0.05	
$FeSi_x$ ($x\approx2$) (RT deposited) 90 Å	Fe-Si	2.34±0.02	8±0.5	0.04	0.36±0.02
	Fe-Fe	2.69±0.02	3.4±0.5	0.03	
$FeSi_x$ ($x\approx1.6$) (RT depostied) 90 Å	Fe-Si	2.37±0.02	8±0.5	0.06	0.38±0.02
	Fe-Fe	2.74±0.04	4.0±1	0.05	
FeSi (RT deposited) 50 Å	Fe-Si	2.36±0.02	8±0.5	0.06	0.40±0.02
	Fe-Fe	2.75±0.02	6.0±0.5	0.06	
FeSi (RT deposited) 90 Å	Fe-Si	2.37±0.02	8±0.5	0.06	0.41±0.02
	Fe-Fe	2.75±0.02	6.0±0.5	0.06	

shows filtered EXAFS data (dots) and fits (full line) for RT-grown FeSi and $FeSi_2$ and for $FeSi_2$ annealed at 600 °C.

C. Discussion

FeSi Fourier-filtered spectra are well accounted for by eight Si neighbors at $R_1=2.36$ Å and six Fe atoms at $R_2=2.75$ Å. The $\Delta R=R_2-R_1$ of 0.40 Å given by the beat node method is in very good agreement with the value of 0.39 Å deduced from simulations. These Fe-Si and Fe-Fe bond lengths have been compared with those deduced from the lattice parameter of FeSi measured by Onda *et al.*[25] Indeed they have measured a lattice parameter $a_{FeSi}=2.77$ Å by x-ray diffraction, resulting in a misfit of ~2% and thus a distortion of the FeSi film. It was shown that FeSi films with thicknesses typically below 70 Å are fully strained. This strain releases continuously above this critical thickness. The 50-Å-thick epitaxial FeSi layer was found to be under compressive strain on the basis of RBS measurements. $\Delta\theta$ measured on this film was $+0.96°$. Similar measurements have not been done for the 90-Å-thick FeSi layer. Nevertheless, on the basis of strain measurements of Ref. 25, the strain release in 90-Å-thick FeSi is expected to be rather small. This is confirmed by EXAFS measurements (Table II) which show only minor differences between Fe-Si and Fe-Fe bond lengths measured on 50- and 90-Å-thick FeSi layers. In a perfect cubic CsCl-type FeSi, Fe-Si and Fe-Fe bond lengths would be $R_1=2.40$ Å and $R_2=2.77$ Å, respectively. When epitaxially grown on Si(111), R_1 and R_2 must be modified. In particular, the eight Si NN bond lengths are no longer equivalent, and one would expect six Si atoms at 2.36 Å, with a bond angle of ~69.8° with respect to the normal to the sample, and two Si atoms at 2.44 Å with Fe-Si bonds perpendicular to the surface. At magic incidence ($\psi=54°$) the weighted mean Fe-Si bond length would be $\langle R_1\rangle=2.38$ Å, thus shorter than in a perfect CsCl crystal. Fe-Fe bond lengths are also expected to decrease at a value $\langle R_2\rangle=2.75$ Å. Fe-Si and Fe-Fe bond lengths deduced from EXAFS simulations are in fairly good agreement with those extracted from structural parameters given in Ref. 25. Furthermore, coordination numbers deduced from EXAFS fits are compatible with those expected for a cubic CsCl-type structure, Fe atoms being coordinated with eight Si atoms at 2.36 Å and six Fe atoms at 2.75 Å.

Upon decreasing the Fe-to-Si ratio in the RT-deposited films, Fe-Si and Fe-Fe bond lengths along with Fe coordination numbers decrease as shown in Table II. The difference ΔR between Fe-Fe and Fe-Si bond lengths also decreases continuously when the silicide becomes richer in Si, as evidenced in Fig. 6. For a 1:2 ratio, experimental data are well accounted for by eight Si atoms at $R_1=2.34$ Å and ~3 Fe atoms at $R_2=2.69$ Å. In the high-temperature-annealed $FeSi_2$ film, the structural order in the 2–3-Å range around a given Fe atom is improved, as evidenced by $\Delta\sigma$ values with respect to $CoSi_2$, which are close to zero. It shows that the 600 °C annealed silicide crystallinity is close to that of well-crystallized $CoSi_2$. Fe-Si and Fe-Fe bond lengths are close to the ones measured on RT-deposited $FeSi_x$ ($x\sim2$). Let us again compare these bond lengths with those deduced from x-ray diffraction.[4,25] For an Fe disilicide the situation is more complicated than for FeSi. As a matter of fact the Si-rich silicide structure was found to depend on the preparation conditions. It has been shown in Ref. 25 that $FeSi_2$ grown by RT codeposition on Si(111) also crystallizes in a CsCl-type structure. It was proposed that, in order to preserve the 1:2 Fe-to-Si ratio, Fe vacancies are randomly distributed over the silicide film. The lattice parameter inferred from x-ray diffraction was found to be 2.70 Å. Using the RBS technique, it was shown that these RT-deposited films are under tensile (instead of compressive for FeSi) strain, with $\Delta\theta=-0.28°$. Taking into account the lattice distortion, one would expect the following first-shell coordination radii around a given Fe atom: six Si atoms at 2.33 Å, two Si atoms at 2.35 Å, and three Fe atoms at a mean distance of $\langle R_2\rangle=2.70$ Å. For EXAFS performed at magic incidence ($\psi=54°$), $\langle R_1\rangle$ and $\langle R_2\rangle$ are expected to be 2.34 and 2.70 Å, respectively. Alternatively, an α-$FeSi_2$-derived structure has been proposed by Jedrecy *et al.*[4] for $FeSi_2$ silicides grown either by solid-phase epitaxy or by metal-organic chemical-vapor deposition. The main differences between true α-$FeSi_2$ and α-$FeSi_2$-derived structures are, first, a random distribution of ~15–20 % of the Fe atoms located in the Si parallelepipeds of Fig. 1 over the unoccupied ones; and, second, a large change of lattice parameters. In Ref. 4 they are $a'=5.377$ Å and $c'=5.458$ Å instead of $a=2.695$ Å and $c=5.134$ Å for the true α-$FeSi_2$ structure. The α-$FeSi_2$-derived structure would give rise to a value $\langle R_1\rangle=2.34$ Å and $\langle R_2\rangle=2.70$ Å, very close to that expected for a cubic CsCl-type structure. Thus Fe-Si and Fe-Fe bond lengths of $R_1=2.34$ Å and $R_2=2.69$ Å, along with Si and Fe first-neighbor numbers deduced from EXAFS measurements, are compatible with both CsCl- and α-$FeSi_2$-derived structures. This is not surprising since, in both structures, Fe atoms reside in a very similar environment.

Interestingly, more information can be extracted from FT spectra of Figs. 4 and 5. As opposed to FeSi, the RT-grown $FeSi_x$ ($x\sim2$) FT spectrum shown in Fig. 4 indicates that scatterers located at distance larger than 3 Å contribute very weakly to the EXAFS signal. In agreement with LEED experiments, this effect could be due to the poorer crystallinity of the $FeSi_x$ ($x\sim2$) film. However, XPD spectra of Fig. 2 indicate that these Si-rich silicides are ordered enough to give Fe $2p_{3/2}$ core-level intensity modulations comparable to that of FeSi. XPD is expected to have a shorter coherence length than LEED, but scatterers at distances larger than 3 Å must be taken into account to explain the intensity maxima at ~30°. The conclusions inferred from XPD and EXAFS seem contradictory. However, the information extracted from XPD and EXAFS is not similar but rather complementary. Indeed XPD profiles reflect mainly bond angles, while EXAFS gives essentially bond lengths. In order to test if this effect is related or not to the silicide crystallinity, let us look at the high-temperature-annealed $FeSi_2$ FT shown in Fig. 4. This FT spectrum is very similar to that

of RT-grown $FeSi_x$ ($x \sim 2$). The first-neighbor peak is enhanced with respect to the RT ones due to the improvement of the silicide crystallinity. As pointed out previously, this improvement is evidenced by a 2×2 LEED pattern and σ values extracted from EXAFS treatments very close to that measured for $CoSi_2$. However, the atomic arrangement at distances of 3–6 Å is not improved by high-temperature annealing, as evidenced by the lack of FT maxima in this region. Thus at this stage one might conclude that the very weak contribution of scatterers more than 3 Å from the emitter to the $FeSi_2$ FT arises from a deviation from CsCl or α-$FeSi_2$ structures rather than from silicide crystalline quality.

Among other possible causes of the lack of peaks above 3 Å, one might consider deviations from perfect cubic or quadratic crystalline structures due to the effect of epitaxial strain. Nevertheless a lattice distortion of CsCl or α-$FeSi_2$ along the [111] axis of the Si(111) substrate induced by epitaxy cannot alone explain the lack of FT maxima in the 3–6-Å region, since it can be also observed for FeSi and $CoSi_2$. As a matter of fact, the coordination polyhedron deformation induced by epitaxy is expected to be similar in FeSi and $FeSi_2$. Maxima are observed at distances larger than 3 Å in RT-grown FeSi, $CoSi_2$, and ε-FeSi (Fig. 5). Well-defined maxima are not observed for $FeSi_2$, suggesting that a distortion of the cubic structure. For instance, Fig. 4 shows that $FeSi_2$ FT's are very similar to that of β-$FeSi_2$, in the sense that peaks above 3 Å are missing in both cases. As pointed out previously, β-$FeSi_2$ can be thought of as a distorted CaF_2 structure in which the Fe emitter resides in two inequivalent sites, with numerous inequivalent Si and Fe neighbors arising from lattice distortion. However, a similar lattice distortion would also result in the absence of XPD modulations typical of a cubic local arrangement in RT-grown and high-temperature annealed $FeSi_x$ ($x \sim 2$). Actually, a more likely explanation is that in both structural models proposed in Refs. 4 and 25, CsCl- and α-$FeSi_2$-derived lattices, there are randomly distributed Fe vacancies which yield a broadening of the distribution of Fe-Fe distances, and result in the lack of the peak around 3.5 Å.

IV. CONCLUSION

Using EXAFS combined with XPD, LEED, and IMEED techniques, we have characterized the local order in codeposited metastable Fe silicides. We have confirmed that Fe environment in RT-grown FeSi is in good agreement with a cubic CsCl-type FeSi structure. For silicide grown with a 1:2 Fe-to-Si stoichiometry, the Fe-Si and Fe-Fe bond lengths are compatible with proposed CsCl- or α-$FeSi_2$-derived structures. Large $FeSi_2$ domains can be grown epitaxially on Si(111), but with a substantial amount of disorder due to randomly distributed iron vacancies. The structure of these silicides, when prepared in the present conditions, is definitively different from the CaF_2-type γ-$FeSi_2$ structure.

[1]J. Chevrier, V. Le Thanh, S. Nitsche, and J. Derrien, Appl. Surf. Sci. **56-58**, 438 (1992).

[2]X. W. Lin, M. Behar, J. Desimoni, H. Bernas, J. Washburn, and Z. Liliental-Weber, Appl. Phys. Lett. **63**, 105 (1993).

[3]J. Chevrier, P. Stocker, V. Le Thanh, J. M. Gay, and J. Derrien, Europhys. Lett. **22**, 449 (1993).

[4]N. Jedrecy, A. Waldhauer, M. Sauvage-Simkin, R. Pinchaux, and Y. Zheng, Phys. Rev. B **49**, 4725 (1994).

[5]F. Sirotti, M. De Santis, X. Jin, and G. Rossi, Phys. Rev. B **49**, 11 134 (1994).

[6]N. Onda, H. Sirringhaus, S. Goncalves-Conto, C. Schwarz, S. Zehnder, and H. von Känel, Appl. Surf. Sci. **73**, 124 (1993).

[7]N. Cherief, R. Cinti, M. de Crescenzi, J. Derrien, T. A. Nguyen Tan, and J. Y. Veuillen, Appl. Surf. Sci. **41/42**, 241 (1989), and references therein.

[8]A. Rizzi, H. Moritz, and H. Lüth, J. Vac. Sci. Technol. A **9**, 912 (1991).

[9]M. De Creszenzi, G. Gaggiotti, N. Motta, F. Patella, A. Balzarotti, and J. Derrien, Phys. Rev. B **42**, 5871 (1990).

[10]D. J. Oostra, D. E. W. Vandenhoudt, C. W. T. Bulle-Lieuwma, and E. P. Naburgh, Appl. Phys. Lett. **59**, 1737 (1991).

[11]K. Radermacher, S. Mantl, Ch. Dieker, and H. Lüth, Appl. Phys. Lett. **59**, 2145 (1991).

[12]X. Wallart, H. S. Zeng, J. P. Nys, and G. Dalmai, Appl. Surf. Sci. **56-58**, 427 (1992).

[13]U. Kafader, P. Wetzel, C. Pirri, and G. Gewinner, Appl. Phys. Lett. **63**, 2360 (1993).

[14]H. Sirringhaus, N. Onda, E. Müller-Gubler, P. Müller, R. Stalder, and H. von Känel, Phys. Rev. B **47**, 10 567 (1993).

[15]N. Jedrecy, Y. Zheng, A. Waldhauer, M. Sauvage-Simkin, and R. Pinchaux, Phys. Rev. B **48**, 8801 (1993).

[16]H. von Känel, R. Stalder, H. Sirringhaus, N. Onda, and J. Henz, Appl. Surf. Sci. **43**, 196 (1991).

[17]A. L. Vazquez de Parga, J. De la Figuera, C. Ocal, and R. Miranda, Europhys. Lett. **18**, 595 (1992).

[18]J. Alvarez, A. L. Vazquez de Parga, J. J. Hinarejos, J. De la Figuera, E. G. Michel, C. Ocal, and R. Miranda, J. Vac. Sci. Technol. A **11**, 929 (1993).

[19]M. G. Grimaldi, G. Franzo, S. Ravesi, A. Terrasi, G. Spinella, and A. La Mantia, Appl. Surf. Sci. **74**, 19 (1994).

[20]H. von Känel, K. A. Mäder, E. Müller, N. Onda, and H. Sirringhaus, Phys. Rev. B **45**, 13 807 (1992).

[21]N. Onda, J. Henz, E. Müller, K. A. Mäder, and H. von Känel, Appl. Surf. Sci. **56-58**, 421 (1992).

[22]U. Kafader, M. H. Tuilier, C. Pirri, P. Wetzel, G. Gewinner, D. Bolmont, O. Heckmann, D. Chandesris, and H. Magnan, Europhys. Lett. **22**, 529 (1993).

[23]U. Kafader, C. Pirri, P. Wetzel, and G. Gewinner, Appl. Surf. Sci. **64**, 297 (1993).

[24]K. Mäder, H. von Känel, and A. Baldereschi, Phys. Rev. B **48**, 4364 (1993).

[25]N. Onda, H. Sirringhaus, S. Goncalves-Conto, C. Schwartz, E. Müller-Gubler, and H. von Känel, in *Evolution of Surface and Thin Film Microstructure Symposium*, edited by H. A. Atwater, E. Chason, M. Grabow, and M. Lagally, MRS Symposia Proceedings No. 280 (Materials Research Society, Pittsburgh, 1993), p. 581.

[26]S. A. Chambers, Surf. Sci. Rep. **16**, 261 (1992).
[27]A. Michalovicz, *Logiciels pour la Chimie* (Société Francaise de Chimie, Paris, 1991), p. 102.
[28]P. Villars and L. D. Calvert, *Pearson's Handbook of Crystallographic Data for Intermetallic Phases* (American Society of Metals, Metals Park, OH, 1985).
[29]Z. Tan, F. Namavar, J. I. Budnick, F. H. Sanchez, A. Fashihuddin, S. M. Heald, C. E. Bouldin, and J. C. Woicik, Phys. Rev. B **46**, 4077 (1992).
[30]A. G. McKale, B. W. Veal, A. P. Paulikas, S. K. Chan, and G. S. Knapp, J. Am. Chem. Soc. **110**, 3763 (1988).
[31]P. A. Lee and G. Beni, Phys. Rev. B **15**, 2862 (1977).
[32]G. Martens, P. Robe, N. Schwentner, and A. Werner, Phys. Rev. Lett. **39**, 1411 (1977).
[33]A. Balzarotti, F. Comin, L. Incoccia, S. Mobilio, M. Piacentini, and A. Savoia, in *Inner-Shell and X-ray Physics of Atoms and Solids,* edited by D. J. Fabian, H. Kleinpoppen, and L. M. Watson (Plenum, New York, 1981), p. 723.
[34]H. S. Zeng, X. Wallart, J. P. Nys, G. Dalmai, and P. Friedel, Phys. Rev. B **44**, 13 811 (1991).
[35]H. von Känel, Mater Sci. Rep. **8**, 193 (1992).